Cryst. Res. Technol. **47**, No. 2, 195 – 201 (2012) / **DOI** 10.1002/crat.201100614

Substrate effect on microstructure and optical performance of sputter-deposited TiO_2 thin films

G. Yildirim*[1], S. Bal[1], M. Gulen[1], A. Varilci[1], E. Budak[2], and M. Akdogan[1]

[1] Abant Izzet Baysal University, Department of Physics, Bolu 14280, Turkey
[2] Abant Izzet Baysal University, Department of Chemistry, Bolu 14280, Turkey

Received 14 December 2011, revised 16 January 2011, accepted 18 January 2012
Published online 31 January 2012

Key words TiO_2 thin films, DC sputter, XRD, AFM, UV-Vis spectra.

This study deals with the role of the different substrates on the microstructural, optical and electronical properties of TiO_2 thin films produced by conventional direct current (DC) magnetron sputtering in a mixture of pure argon and oxygen using a Ti metal target with the aid of X–ray diffractometer (XRD), ultra violet spectrometer (UV–vis) and atomic force microscopy (AFM) measurements. Transparent TiO_2 thin films are deposited on Soda lime glass, MgO(100), quartz and sitall substrates. Phase purity, surface morphology, optical and photocatalytic properties of the films are compared with each other. It is found that the amplitude of interference oscillation of the films is in a range of 77-89%. The transmittance of the film deposited on Soda lime glass is the smallest while the film produced on MgO(100) substrate obtains the maximum transmittance value. The refractive index and optical band gap of the TiO_2 thin films are also inferred from the transmittance spectra. The results show that the film deposited on Soda lime glass has the better optical property while the film produced on MgO(100) substrate exhibits much better photoactivity than the other films because of the large optical energy band gap. As for the XRD results, the film prepared on MgO(100) substrate contains the anatase phase only; on the other hand, the other films contain both anatase and rutile phases. Furthermore, AFM images show that the regular structures are observed on the surface of all the films studied.

1 Introduction

Titanium dioxide or titania (TiO_2) film is one of the most widely studied transition-metal oxides. During the past few decades, the TiO_2 films have attracted great attention for their potential applications in physical, optical, electrical, photocatalytic and electronic fields [1-11]. A variety of techniques such as chemical spray pyrolysis [12], chemical vapor deposition [13,14], sol–gel [15], sputtering [6,16], and electron-beam evaporation [17,18] have been used to prepare high quality TiO_2 thin films. The conventional sputtering methods, among others, are the most preferred technique owing to the reproducible deposition of the films accomplished quite easily compared to the other methods.

The TiO_2 film exhibits three distinct polymorphs: the rutile phase, the anatase phase and the brookite phase. Among these phases, although the rutile structure is the most common in nature, the anatase structure is usually used as photocatalyst because of the large optical band gap energy, about 3.2 eV, related to an indirect band to band electronic transition [19,20]. As well known less electron–hole recombination is observed in indirect band gap materials, leading to the use of the anatase structure as wide band gap semiconductor, specifically for the charge separation in dye-sensitized solar cell [20,21]. Nevertheless, the large band gap limits the photocatalytic efficiency of the TiO_2 film under sunlight irradiation due to the use of only 2–3% of the UV light in the total solar spectrum for water splitting. Several methods such as the chemical doping (metals, rare elements, nitrogen or iron), and the change of annealing conditions (ambient temperature, deposition time, substrate temperature) and sputtering parameters (RF or DC gun power, sputtering pressure and Ar to O_2 gas ratio) have

* Corresponding author: e-mail: yildirim_g@ibu.edu.tr

therefore been studied to increase both the photocatalytic efficiency of the TiO_2 structures [22,23] and the surface area and the surface hydrophilicity [24]. The required surface area and hydrophilicity properties of the TiO_2 film are obtained from the small grain/particles size in anatase structure, resulting in a not only more efficient light and water absorption but higher photoefficiency and photocatalytic activity [25], as well.

In the present study, we report the effect of the various substrates on the microstructural, optical and electronical properties of the TiO_2 thin films fabricated by DC sputtering method. Optical and photocatalytic properties of the films in this work are investigated by ultra violet spectrometer (UV–vis); phase purity and crystallinity data are examined by means of the X–ray diffractometer (XRD) and the microstructural properties and height asymmetries are analyzed by atomic force microscopy (AFM) measurements. Optical energy band gaps, porosities and refraction indices inferred from transmittance spectra are also discussed.

2 Experimental

Titanium dioxide films are deposited on soda lime glass, MgO(100), quartz and sitall substrates by reactive DC magnetron sputtering method (NSC–3000 DC Sputter Machine). Prior to coating, all the substrates are ultrasonically cleaned by acetone and washed thoroughly with deionized water and then dried by way of nitrogenous gas. Thus, the substrates are ready for sputtering process. Titanium disc (99.9% pure) with a 50 mm diameter and a 2 mm thickness is used as sputtering target. The distance between the target and substrate is adjusted to be about 50 mm. The substrates prepared are placed on a hot plate (450 °C) in a vacuum chamber evacuated to a pressure lower than 10^{-6} Pa for the film fabrication. All the samples are reactively sputtered in a mixture of 99.999% pure argon (30 sscm for sputtering gas) and 99.99% pure oxygen (30 sscm for reactive gas). 250 W DC power is applied between the target and substrates for 3 h at 450 °C. The TiO_2 samples produced by in-situ annealing method on the different substrates such as soda lime glass, sitall, quartz and MgO(100) will hereafter be denoted as Ti-0, Ti-1, Ti-2 and Ti-3, respectively.

The crystal structures of the TiO_2 films studied are characterized by XRD investigation by means of a Rigaku Multiflex XRD with CuK_α radiation (λ=1.5418 Å) in the range 2θ=20–50° at a scan speed of 3°/min and a step increment of 0.02° at room temperature. Furthermore, the average sizes of the crystal of the samples are estimated from the Scherrer–Warren approach by utilizing from the broadening nature of the XRD peaks. Moreover, the transmittance spectra of the films are recorded in the wavelength range from 300 to 700 nm by a JASCO 430 UV–VIS spectrophotometer; however, we did not measure the transmittance spectrum of the Ti-1 sample. The refractive index (n_λ), porosity and optical band gap energy values of the TiO_2 films fabricated are also calculated with the aid of the transmittance spectra. Additionally, the microstructural properties and height asymmetries of the films are conducted using AFM from Nanomagnetic Instruments.

3 Results and discussion

X–ray diffraction patterns Figure 1 indicates the x–ray diffraction patterns between 20° and 50° for the thin films prepared. The anatase peaks are presented by A(*hkl*) Miller indices while the peaks of rutile phase are shown by R(*hkl*) Miller indices given in the diagrams. It is found that, no secondary phase containing Ti element or any other cation is observed for all the samples studied. Moreover, the Ti-3 sample illustrates the highest peak intensities belonging to anatase phase whereas the rutile phase is found to be denser than other phase in the Ti-0 sample. Additionally, the Ti-3 sample can be characterized as nanocrystalline anatase and the grain size of that film is determined from the anatase (101) peak using Scherrer's equation [26-30]. According to the equation, in broadening region the average size of a crystal is defined as;

$$d = \frac{0.941\lambda}{B\cos\theta_B}, \tag{1}$$

where d is the thickness of the crystal, λ is the wavelength, B is the fullwidth half maximum (FWHM) of the Bragg peak corrected using the corresponding peak in micron-sized powder and θ_B is the Bragg angle, also. B

is the line broadening, by reference to a standard, so that

$$B^2 = B_m^2 - B_s^2 , \tag{2}$$

where B_s is the half-width of the standard material in radians. The calculations obtained give that the largest grain size (45 nm) is obtained for the Ti-0 sample (Table 1).

Table 1 Comparative results of TiO_2 thin films prepared on Soda lime glass, sitall, quartz and MgO(100) substrates.

Parameters	Ti-0	Ti-1	Ti-2	Ti-3
Grain size from XRD (nm)	45	38	26	17
Grain size from AFM (nm)	52	45	36	23
Refraction index	2.08	—	1.97	1.83
Porosity (%)	56.12	—	46.24	37.78
Optical Band gap energy (eV)	2.92	—	3.06	3.20

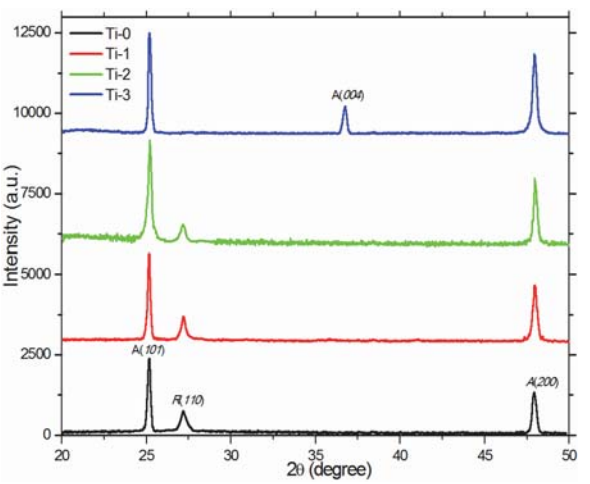

Fig. 1 XRD patterns of the Ti-0, Ti-1, Ti-2 and Ti-3 samples (A shows anatase phase while R presents rutile phase).

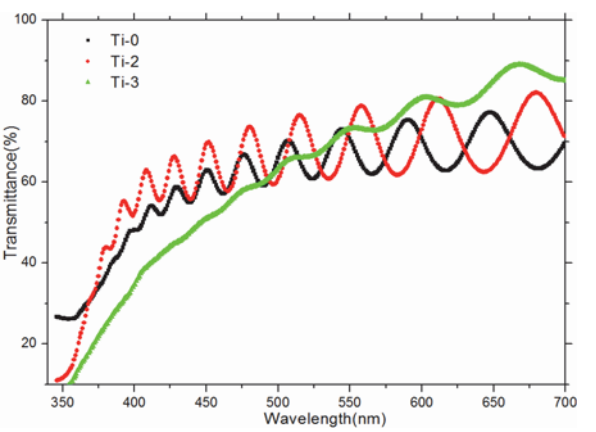

Fig. 2 Optical transmittance spectra of TiO_2 thin films deposited on Soda lime glass, quartz and MgO(100) substrates.

Transmittance spectra Homogeneity, porosity and refraction index of a film can be determined by transmittance spectra, such that high transmittance of the film indicates its low surface roughness, low refraction index, high porosity and good homogeneity [31,32]. Figure 2 depicts the transmittance spectra as a function of wavelength in the wavelength range 300–700 nm for TiO_2 thin films prepared using the different substrates except for the Ti-1 sample due to the fact that we did not measure the transmittance of that film. It is apparent from the figure that the amplitude of interference oscillation of the thin films is obtained to be in a range of 77-89%. The maximum transmittance is observed to be 89% for the Ti-3 sample whereas the Ti-0 film is found to obtain the minimum transmittance value (77%). A considerable reduction in transmittance is attributable to the growth of particles, supported by both XRD and AFM results. Therefore, Ti-0 has better optical property than the other films studied.

Refractive index and porosity analyses The refractive index (n_λ) and porosity of the TiO_2 films prepared using different substrates are tabulated in table 1. The former is calculated from the optical transmittance data by means of the Swanepoel's envelope method [33], which is based on the analysis of the transmittance spectrum of a weakly absorbing film deposited on a non-absorbing substrate [34]. Hence, the refractive index (n_λ) over the spectral range is deduced from the envelopes fitted to the extrema measured:

$$n_\lambda = \left[N + (N^2 - n_0^2 n_1^2)^{1/2} \right]^{1/2} \tag{3}$$

$$N = 2n_0 n_1 \left[(T_{M(\lambda)} - T_{m(\lambda)}) / T_{M(\lambda)} T_{m(\lambda)} \right] + (n_0^2 + n_1^2)/2 , \tag{4}$$

where $T_{M(\lambda)}$ and $T_{m(\lambda)}$ are the transmittance maximum and minimum of the film at a wavelength λ; n_0 is the refractive index of air and n_1 is the refractive index of the substrates, respectively. The films prepared are assumed as homogeneous structures in calculation. However, the refractive index could not be calculated for Ti-1 sample because we did not record the transmittance spectrum. Table 1 indicates that the calculated refractive indices of the films (except for Ti-1 sample) are observed to be in a range of 1.83-2.08. Among the TiO_2 films studied, the Ti-0 (Ti-3) is found to obtain the maximum (minimum) refractive index. This phenomenon may be explained by the variation of the oxygen in the TiO_2 films [35-37]. Moreover, the latter (porosity of the TiO_2 films) is calculated with the aid of the following equation [38]:

$$\text{Porosity} = (1 - \frac{n^2 - 1}{n_d^2 - 1}) \times 100(\%), \tag{5}$$

where the n_d is 2.52 (the refractive index of pore-free anatase) [39] when the n is the refractive index of the porous thin films. The porosity values calculated are also given in table 1. It is visible from the table that the maximum (minimum) porosity is found to be about 56.1% (37.8%) for the Ti-3 (Ti-0) sample, supported by AFM images. According to the result, the Ti-3 sample is more porous than the other films fabricated in this work, showing that both the transmittance and porosity tend to reduce with the decrease of the anatase phase; or the increase of the rutile phase in the sample. Indeed, the significant change of the phase formation is observed from the XRD investigations. To sum up, the substrate effect on the transmittance spectra, refractive index and porosity of the TiO_2 films is clearly obtained.

Band gap energies There are considerable models and reports to find the absorption coefficient and optical band gap energy (E_g) [40]. In the present work, we assume an indirect transition (value of the energy separation between the top of the valence band and the bottom of the conduction band) for the determination of the optical band gap of the films by means of the following relation [41]:

$$\alpha(h\nu) \infty A(h\nu - E_g)^2, \tag{6}$$

where α is absorption coefficient when A is the edge width parameter and hν is the photon energy. Figure 3 illustrates $(\alpha h\upsilon)^2$ versus photon energy (eV) plots for the Ti-0, Ti-2, and Ti-3, respectively. The band gap values of the films are deduced from the extrapolation of the linear plots of $(\alpha h\nu)^{1/2}$ versus hν when (α = 0). The energy gap is found to be about 2.92 eV for the Ti-0, 3.06 eV for the Ti-2 and 3.20 eV for the Ti-3 sample, respectively. Based on these results, the energy band gap for the Ti-3 sample is obtained to shift to higher energy value, associated with the decrease of the grain size indicative of the presence of the quantum confinement effect [42-46].

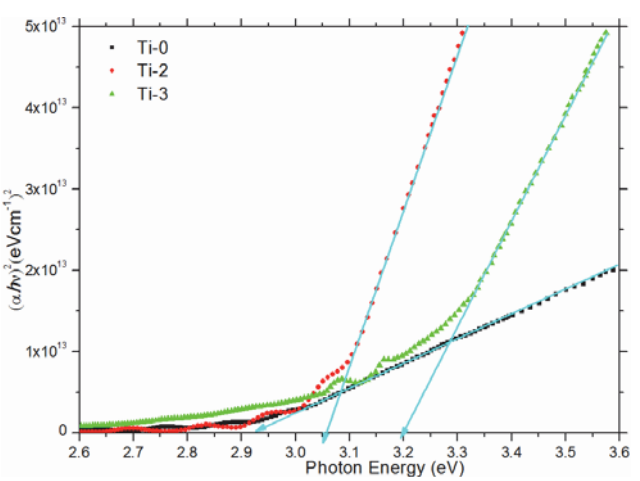

Fig. 3 Optical absorption coefficient α versus band gap energy (E_g) of TiO_2 thin films.

Surface morphology Surface morphology of the TiO_2 films prepared in this study is conducted using AFM technique. Thickness, grain size, average roughness and rms roughness are important parameters to obtain about the microstructural properties of a thin film. Thickness and grain size values of the films are found

with the aid of AFM images in figure 4. The obtained results are depicted in table 2. One can observe from the table, the thickness values of the films are about 100 nm except for the Ti-2 sample (70 nm); on the other hand, the maximum grain size of 52 nm is obtained for the Ti-0 sample as against 24 nm (minimum size) for the Ti-1 sample, supported by XRD results. Moreover, average roughness parameter (S_a) is the arithmetic mean or average of the absolute distances of the surface points from the mean plane while rms roughness parameter (S_q) is the root mean square of the surface departures from the mean plane within the sampling area [47]. Average roughness parameters can be calculated by means of the following relation:

$$S_a = \frac{1}{MN}\sum_{j=1}^{N}\sum_{i=1}^{M}|z|(x_i, y_j) \tag{7}$$

and rms roughness parameter can be calculated using the equation,

$$S_q\sqrt{\frac{1}{MN}\sum_{j=1}^{N}\sum_{i=1}^{M}z^2(x_i, y_j)}\,, \tag{8}$$

where M is the number of columns in the surface and N is the number of rows in the surface.

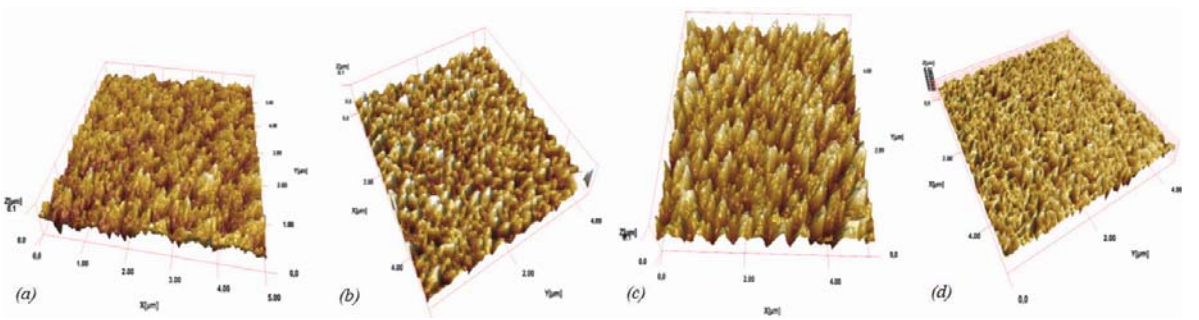

Fig. 4 Atomic Force Microscopy images of TiO2 film deposited on (a) Soda lime glass, (b) quartz, (c) MgO(100) and (d) sitall substrates.

Table 2 Statistical parameters of the Ti-0, Ti-1, Ti-2 and Ti-3 films.

Statistical Parameters	Ti-0	Ti-1	Ti-2	Ti-3
Average roughness (nm)	70.4	39.5	47.9	95.7
RMS roughness (nm)	72.1	40.7	48.7	98.5
Skewness, S_{sk}	1.067	1.091	1.039	1.076
Kurtosis, S_{ku}	1.179	1.255	1.099	1.201

The results obtained are given in table 2. It is found that the Ti-3 sample obtains the highest surface roughness (S_a: 95.7 nm and S_q: 98.5 nm) among the films produced while the smallest values are noted for the Ti-1 sample. According to these results, the regular structures were observed on the surface of the films studied. However, the different surface roughness values might show the possible reason for the variation of the oxygen in the samples studied in this work.

The statistical analysis of AFM image is also carried out by using the height distribution histogram depicted in figure 5. The height asymmetry can be explained by the surface skewness and kurtosis from the quantitative surface roughness parameters [48]. The surface skewness (s_{sk}) is a measurement for the symmetry of the variation of a surface about its mean plane. Whenever a Gaussian surface obtains a symmetrical shape for the height distribution, the surface skewness is zero. A plateau honed surface with predominant plateau and deep valleys tend to have a negative skewness whereas a surface comprised of disproportionate peaks obtains positive skewness value. The skewness can be computed from the following relation:

$$S_{sk} = \frac{1}{MNS_q^3}\sum_{j=1}^{N}\sum_{i=1}^{M}z^3(x_i, y_j)\,. \tag{9}$$

On the other hand, the surface kurtosis (s_{ku}) is a measurement of the peakedness or sharpness of a surface. For a Gaussian surface, the kurtosis value is 3. If a surface is centrally distributed kurtosis value is greater than 3.

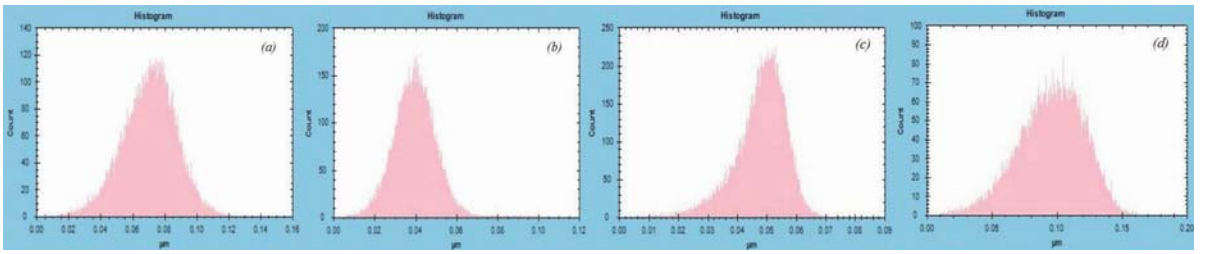

Fig. 5 Height distribution histogram of the samples produced on (a) Soda lime glass, (b) quartz, (c) MgO(100) and (d) sitall substrates.

When a surface has a well spread out distribution, the kurtosis value is less than 3. Kurtosis is calculated using the following equation:

$$S_{ku} = \frac{1}{MNS_q^4} \sum_{j=1}^{N} \sum_{i=1}^{M} z^4(x_i, y_j) . \tag{10}$$

The surface skewness and kurtosis roughness of the samples are also listed in table 2. It is visible from the table that the surface skewness is obtained to be positive for all the samples while the surface kurtosis is found to be less than 3. According to the combination of the skewness and kurtosis values, the film surfaces are found to be spread out distribution and comprised of disproportionate number of peaks. Based on the interpretation of the surface morphology and statistical parameters, the films produced in this work can be useful for applications in technology and industry.

4 Conclusion

In this study, it is analyzed that how the substrate affects the microstructural, optical and electrical properties of TiO_2 thin films by means of the X–ray diffractometer (XRD), ultra violet spectrometer (UV–vis) and atomic force microscopy (AFM) measurements. The results indicate that all the films prepared have the similar microstructural features; however, the optical and electrical properties of the films are found to be different from each others and so the following statements are concluded:

- The film thickness values are observed to be about 100 nm except the Ti-2 sample (70 nm); on the other hand, the maximum grain size of 52 nm is obtained for the Ti-0 sample as against 23 nm (minimum size) for the Ti-3 sample.
- The Ti-3 sample having only anatase phase peaks such as A(101), A(004) and A(200) obtains the largest peak intensity among the samples prepared. Moreover, the A(004) peak intensity disappears completely in the other samples. Rutile phase is also observed in the Ti-1, Ti-2 and especially Ti-0 samples.
- The transmittance of the Ti-0 film is noticed to be the smallest (77%) while the Ti-3 sample is obtained to have the maximum transmittance value (89%) as a result of the different particle sizes.
- The Ti-0 (Ti-3) sample is observed to obtain the maximum (minimum) refractive index computed from the Swanepoel's envelope method.
- The Ti-3 sample is obtained to be more porous while the Ti-0 sample is noted to be denser than the other samples fabricated in this work.
- The optical band gap is found to be about 2.92 eV (smallest) for the Ti-0, 3.06 eV for the Ti-2 and 3.20 eV (greatest) for the Ti-3 sample.

Acknowledgements This work was supported by The Research Fund of Abant Izzet Baysal University, BOLU, Turkey, under contract No. 2011.03.02.434.

References

[1] M. Zribi, M. Kanzari, and B. Rezig, Thin Solid Films **516**, 1476 (2008).
[2] K. Kato, A. Tsuzuki, H. Taoda, Y. Torii, T. Kato, and Y. Butsugan, J. Mater. Sci. **30**, 837 (1995).

[3] A. I. Al-Homoudi, J. S. Thakur, R. Naik, G. W. Auner, and G. Newaz, Appl. Surf. Sci. **253**, 8607 (2007).
[4] E. György, G. Socol, E. Axente, I. N. Mihailescu, C. Ducu, and S. Ciuca, Appl. Surf. Sci. **247**, 429 (2005).
[5] E. György, E. Axente, I. N. Mihailescu, C. Ducu, and H. Du, Appl. Surf. Sci. **252**, 4578 (2006).
[6] L. Miao, P. Jin, K. Kanekko, A. Terai, N. Nabatova-Gabain, and S. Tanemura, Appl. Surf. Sci. **212**, 255 (2003).
[7] D. Yoo, Kim, S. Kim, C. H. Hahn, C. Lee, and S. Cho, Appl. Surf. Sci. **253,** 3888 (2007).
[8] B. O. Regan and M. Gratzel, Nature **353**, 737 (1991).
[9] Y. Sato, H. Akizuki, T. Kamiyama, and Y. Shigesato, Thin Solid Films **516**, 5758 (2008).
[10] S. Murugesan, P. Kuppusami, N. Parvathavarthini, and E. Mohandas, Surf. Coat. Technol. **201**, 7713 (2007).
[11] J. Osterwalder, T. Droubay, T. Kaspar, J. Williams, C. M. Wang, and S. A. Chambers, Thin Solid Films **484**, 289 (2005).
[12] M. O. Abou–Helal and W. T. Seeber, Appl. Surf. Sci. **195**, 53 (2002).
[13] A. Brevet, F. Fabreguette, L. Imhoff, M. C. Marco de Lucas, O. Heintz, L. Saviot, M. Sacilotti, and S. Bourgeois, Surf. Coat. Technol. **151–152**, 36 (2002).
[14] G. S. Hermann, Y. Gao, T. T. Tran, and J. Osterwalder, Surf. Sci. **447**, 201 (2000).
[15] S. Sen, S. Mahanty, S. Roy, O. Heintz, S. Bourgeois, and D. Chaumont, Thin Solid Films **474**, 245 (2005).
[16] B. Hunsche, M. Vergöhl, and A. Ritz, Thin Solid Films **502**, 188 (2006).
[17] Y. L. Wang and K. Y. Zhang, Surf. Coat. Technol. **140**, 155 (2001).
[18] S. H. Oh, D. J. Kim, S. H. Hahn, and E. J. Kim, Mater. Lett. **57**, 4151 (2003).
[19] J. Pascual, J. Camassel, and H. Mathieu, Phys. Rev. Lett. **39**, 1490 (1977).
[20] S. Banerjee, J. G. Gopal, P. Muraleedharan, A. K. Tyagi, and B. Raj, Curr. Sci. **90**, 1378 (2006).
[21] M. C. Ferrara, L. Pilloni, S. Mazzarelli, and L. Tapfer, J. Phys. D **43**, 095301 (2010).
[22] Y. Zhang, X. Ma, P. Chen, and D. Yang, J. Cryst. Growth **300**, 551 (2007).
[23] J. Musil, D. Herman, and J. Sicha, J. Vac. Sci. Technol. A **24**, 521 (2006).
[24] D. Luca, D. Mardare, F. Iacomi, and C. M. Teodorescu, Appl. Surf. Sci. **252**, 6122 (2006).
[25] D. Chen, F. Huang, Yi-B. Cheng, and R. A. Caruso, Adv. Mater. **21**, 2206 (2009).
[26] J. Economy and R. Anderson, Inorg. Chem. **5**, 989 (1966).
[27] G. Yildirim, A. Varilci, M. Akdogan, and C. Terzioglu, J. Mater. Sci: Mater. Electron. DOI: 10.1007/s10854-011-0522-7 (2011).
[28] B. D. Cullity, Element of X-ray Diffraction, 3rd Edition (Addition-Wesley, Reading MA, 2001).
[29] S. Bal, M. Dogruer, G. Yildirim, A. Varilci, C. Terzioglu, and Y. Zalaoglu, J. Supercond. Nov. Magn. DOI: 10.1007/s10948-011-1360-9 (2011).
[30] G. Yildirim, S. Bal, E. Yucel, M. Dogruer, M. Akdogan, A. Varilci, and C. Terzioglu, J. Supercond. Nov. Magn. DOI: 10.1007/s10948-011-1324-0 (2011).
[31] R. Thomas, D. C. Dube, M. N. Kamalasanan, and S. Chandra, Thin Solid Films **346**, 212 (1999).
[32] G. Yildirim, M. Akdogan, A. Varilci, and C. Terzioglu, Cryst. Res. Technol. **45**, 1161 (2010).
[33] R. Swanepoel, J. Phys. E **16**, 1214 (1983).
[34] J. C. Manifacier, J. Gasiot, and J. P. Fillard, J. Phys. E **9**, 1002 (1976).
[35] J. K. Yao, Z. X. Fan, Y. X. Jin, Y. A. Zhao, H. B. He, and J. D. Shao, J. Appl. Phys. **102**, 063105 (2007).
[36] J. K. Yao, Z. X. Fan, Y. X. Jin, Y. A. Zhao, H. B. He, and J. D. Shao, Thin Solid Films **516**, 1237 (2008).
[37] J. K. Yao, J. D. Shao, H. B. He, and Z. X. Fan, Appl. Surf. Sci. **253**, 8911 (2007).
[38] B. E. Yoldas and P. W. Partlow, Thin Solid Films **129**, 1 (1985).
[39] W. D. Kingery, H. K. Bowen, and D. R. Uhlmann, Introduction to Ceramics, 2nd Edition (Wiley, NY, 1976).
[40] H. N. Cui, V. Teixeira, and A. Monteiro, Vacuum **67**, 589 (2002).
[41] J. I. Pankove, Optical Processes in Semiconductors, 2nd Edition (Dover Publications Inc., New York, 1970).
[42] Y. D. Glinka, S. H. Lin, L. P. Hwang, Y. T. Chen, and N. H. Tolk, Phys. Rev. B **64**, 085421 (2001).
[43] Y. K. Chang, H. H. Hsieh, W. F. Pong, M. H. Tsai, F. Z. Chien, P. K. Tseng, L. C. Chen, T. Y. Wang, K. H. Chen, D. M. Bhusari, J. R. Yang, and S. T. Lin, Phys. Rev. Lett. **82**, 5377 (1999).
[44] G. L. Tian, H. B. He, and J. D. Shao, Chin. Phys. Lett. **22**, 1787 (2005).
[45] F. M. Liu, T. M. Wang, J. Q. Li, C. Wang, S. K. Zheng, and M. Duan, J. Magn. Magn. Mater. **251**, 245 (2002).
[46] J. T. Jiu, F. M.Wang, and M. Adachi, Mater. Lett. **58**, 3915 (2004).
[47] I. V. Tudose, P. Horvath, M. Suchea, S. Christoulakis, T. Kitsopoulos, and G. Kiriakidis, J. Appl. Phys. **89**, 57 (2007).
[48] C. S. Yadav and P. L. Paulose, New J. Phys. **11**, 103046 (2009).

